

We are IntechOpen, the world's leading publisher of Open Access books Built by scientists, for scientists

6,900

Open access books available

186,000

International authors and editors

200M

Downloads

Our authors are among the

154

Countries delivered to

TOP 1%

most cited scientists

12.2%

Contributors from top 500 universities



WEB OF SCIENCE™

Selection of our books indexed in the Book Citation Index
in Web of Science™ Core Collection (BKCI)

Interested in publishing with us?
Contact book.department@intechopen.com

Numbers displayed above are based on latest data collected.
For more information visit www.intechopen.com



X-Ray Spectroscopy Studies of Iron Chalcogenides

Chi Liang Chen and Chung-Li Dong

Additional information is available at the end of the chapter

<http://dx.doi.org/10.5772/48611>

1. Introduction

A recent study that identified high temperature superconductivity in Fe-based quaternary oxypnictides has generated a considerable amount of activity closely resembling the cuprate superconductivity discovered in the 1980s (Kamihare et al., 2008; Takahashi et al., 2008; Ren et al., 2008). This system is the first in which Fe plays an essential role in the occurrence of superconductivity. Fe generally has magnetic moments, tending to form an ordered magnetic state. Neutron-scattering experiments have demonstrated that mediated superconducting pairing may originate from magnetic fluctuations, similar to our understanding of that in high- T_c cuprates (de la Cruz et al., 2008; Xu et al., 2008). Binary superconductor FeSe_x is another example of a Fe-based superconductor with a less toxic property, leading to the discovery of several superconducting compounds (Hsu et al., 2008). The T_c value of FeSe is ~8 K in bulk form and exhibits a compositional dependence such that T_c decreases for over-doping or under-doping of compounds (McQueen et al., 2009; Wu et al., 2009), as does that of high- T_c cuprates. FeSe has received a significant amount of attention owing to its simple tetragonal symmetry P4/nmm crystalline structure, comprising a stack of layers of edge-sharing FeSe₄ tetrahedron. The phase of FeSe heavily depends on Se deficiency and annealing temperature. While 400 °C annealing reduces the non-superconducting NiAs-type hexagonal phase and increases the PbO-type tetragonal superconducting phase (Hsu et al., McQueen et al., 2009; Wu et al., 2009; Mok et al., 2009), the role of Se deficiency remains unclear. Notably, this binary system is isostructural with the FeAs layer in quaternary iron arsenide. Also, band-structure calculations indicate that FeSe- and FeAs-based compounds have similar Fermi-surface structures (Ma et al., 2009), implying that this simple binary compound may significantly contribute to efforts to elucidate the origin of high-temperature superconductivity in these emerging Fe-based compounds. Therefore, although the electronic structure is of great importance in this respect, spectroscopic measurements are still limited.

According to investigations on how fluorine doping (Kamihara et al., 2008; Dong et al., 2008) and rare earth substitutions (Yang et al., 2009) influence the superconductivity in $\text{LaO}_{1-x}\text{F}_x\text{FeAs}$ compounds, x-ray absorption spectroscopy (Kroll et al., 2008), x-ray photoemission spectroscopy (Malaeb et al., 2008) and resonant x-ray inelastic scattering (Yang et al., 2009) results, Fe $3d$ states hybridize with the As $4p$ states, leading to a situation in which itinerant charge carriers (electrons) are responsible for superconductivity. Most of these studies suggest moderate to weak correlated correlations in this system. Photoemission spectroscopy (PES) measurements (A. Yamasaki et al., 2010) support the density of state (DOS) calculations on the FeSe_x system. These results indicate the Fe-Se hybridization and itinerancy with weak to moderate electronic correlations (Yoshida et al., 2009), while recent theoretical calculations have suggested strong correlations (Aichhorn et al., 2010; Pourret et al., 2011). While fluorine substitution leads to electron doping in the $\text{LaO}_{1-x}\text{F}_x\text{FeAs}$ system, exactly how Se deficiency may bring in the mobile carriers in the FeSe_x system to ultimately lead to superconductivity remains unclear. Therefore, this study elucidates the electronic structure of FeSe_x ($x=1\sim 0.8$) crystals by using XAS Fe and Se K-edge spectra. Powder x-ray diffraction (XRD) measurements confirm the lattice distortion. Analytical results further demonstrate a lattice distortion and Fe-Se hybridization, which are responsible for producing itinerant charge carriers in this system.

As mentioned earlier, although band-structure calculations indicate that FeSe and FeAs-based compounds have similar Fermi-surface structures, the poor quality of crystals arising from serious oxidization at their surfaces inhibit spectral measurements on pure (stoichiometric) FeSe. Also, FeSe exhibits an unstable crystalline structure. Therefore, investigating the effect of chemical substitution, at either the Se or Fe site, is a promising means of maintaining or improving the superconducting behavior on one hand and stabilizing the crystal structure on the other. Te doping of the layered FeSe with the PbO structure modifies its superconducting behavior, with a maximum T_c of ~ 15 K when Te replaces half of the Se. The improvement of T_c , which is correlated with the structural distortion that originates from Te substitution, is owing to the combined effect of lattice disorder, arising from the substitution of larger ions, and electronic interaction. Since layered $\text{FeSe}_{1-y}\text{Te}_y$ crystals are readily cleaved and highly crystalline, x-ray spectra of layered $\text{FeSe}_{1-y}\text{Te}_y$ crystals can provide clearer information about the electronic structure than those of FeSe crystals. Therefore, this study investigates the electronic properties of $\text{FeSe}_{1-y}\text{Te}_y$ ($y=0\sim 1$) single crystals by using XAS and RIXS. XAS is a highly effective means of probing the crystal field and electronic interactions. The excitation-induced energy-loss features in RIXS can reflect the strength of the electron correlation. During their experimental and theoretical work on Fe-pnictides, Yang *et al.* (2009) addressed the issues regarding the Fe-based quaternary oxypnictides. However, few Fe-Se samples of this class have been investigated from a spectroscopic perspective. Angle-resolved photoemission (ARPES) combined with DFT band structure calculation on "11" Fe-based superconductor $\text{FeSe}_{0.42}\text{Te}_{0.58}$ reveals effective carrier mass enhancement, which is characteristic of a strongly electronic correlation (Tamai et al., 2010). This finding is supported by a large Sommerfeld coefficient, ~ 39 mJ/mol K (de la Cruz et al., 2008; Sales et al., 2009) from specific heat measurement. This phenomenon reveals that the FeSe "11" system is regarded as a strongly

correlated system. Moreover, its electronic correlation differs markedly from that of "1111" and "122" compounds, perhaps due to the subtle differences between the p - d hybridizations in the Fe-pnictides and the FeSe "11" system. This postulation corresponds to the observation of p - d hybridization, as discussed later. This postulation is also supported by recent DMFT calculations, which demonstrate that correlations are overestimated largely owing to an incomplete understanding of the hybridization between the Fe d and pnictogen p states (Aichhorn et al., 2009). Nakayama *et al.* (2010) discussed the pairing mechanism based on interband scattering, which has a signature of Fermi surface nesting in ARPES. Based on the SC gap value, their estimations suggest that the system is highly correlated (Nakayama et al., 2010). Moreover, a combined electron paramagnetic resonance (EPR) and NMR study of FeSe_{0.42}Te_{0.58} superconductor has indicated the coexistence of electronic itinerant and localized states (Arçon et al., 2010). The coupling of the intrinsic state with localized character to itinerant electrons exhibits similarities with the Kondo effect, which is regarded as a typical interaction of a strongly correlated electron system. The localized state is characteristic of strong electron correlations and makes the FeSe "11" family a close relative of high- T_c superconductors. Comparing the XAS and RIXS spectra reveals that FeSe_{1-y}Te_y is unlikely a weakly correlated system, thus differing from other Fe-based quaternary oxypnictides. The charge transfer between Se-Te and the Se $4p$ hole state induced by the substitution is strongly correlated with the superconducting behavior. Above results suggest strong electronic correlations in the FeSe "11" system, as discussed later in detail.

2. Experiments

FeSe_x crystals were grown by a high temperature solution method described elsewhere (Wu et al., 2009; Mok et al., 2009). Crystals measuring 5 mm × 5 mm × 0.2 mm with (101) plate like habit could be obtained by this method. Three compositions results of FeSe_x crystals ($x=0.91$, 0.88 and 0.85) are presented here for comparison and clarity. Additionally, large layered single crystals of high-quality FeSe_{1-y}Te_y were grown using an optical zone-melting growth method. Elemental powders of FeSe_{1-y}Te_y were loaded into a double quartz ampoule, which was evacuated and sealed. The ampoule was loaded into an optical floating-zone furnace, in which 2 × 1500 W halogen lamps were installed as infrared radiation sources. The ampoule moved at a rate of 1.5 mm/h. As-grown crystals were subsequently homogenized by annealing at 700 ~800 °C for 48 hours, and at 420 °C and for another 30 hours. Chemical compositions of FeSe_{1-y}Te_y single crystals were determined by a Joel scanning electron microscope (SEM) coupled with an energy dispersive x-ray spectrometer (EDS) (Yeh et al., 2009; Yeh et al., 2008). In the Te substitution series, the composition of nominal $y=0.3$ was FeSe_{0.56}Te_{0.41}; that of nominal $y=0.5$ was FeSe_{0.39}Te_{0.57}; that of nominal $y=0.7$ was FeSe_{0.25}Te_{0.72}, and that of nominal $y=1.0$ was FeTe_{0.91}. The grown crystals were characterized by a Philips Xpert XRD system; T_c was confirmed by both transport and magnetic measurements (Wu et al., 2009; Mok et al., 2009).

X-ray absorption spectroscopy (XAS) provides insight into the symmetry of the unoccupied electronic states. The measurements at the Fe K-edge of chalcogenides were carried out at the 17C1 and 01C Wiggler beamlines at the National Synchrotron Radiation Reach Center

(NSRRC) in Taiwan, operated at 1.5 GeV with a current of 360 mA. Monochromators with Si (111) crystals were used on both the beam lines with an energy resolution $\Delta E/E$ higher than 2×10^{-4} . Absorption spectra were recorded by the fluorescence yield (FY) mode at room temperature by using a Lytel detector (Lytle et al., 1984). All spectra were normalized to a unity step height in the absorption coefficient from well below to well above the edges, subsequently yielding information of the unoccupied states with p character. Standard Fe and Se metal foils and oxide powders, SeO_2 , FeO, Fe_2O_3 and Fe_3O_4 were used not only for energy calibration, but also for comparing different electronic valence states. Since surface oxidation was assumed to interfere with the interpretation of the spectra, the FeSe_x crystals were cleaved *in situ* in a vacuum before recording the spectra.

The unoccupied partial density of states in the conduction band was probed using XAS, while information complementing that obtained by XAS was obtained using XES. Those results reveal the occupied partial density of states associated with the valence band. Detailed x-ray absorption and emission studies were conducted. Next, tuning the incident x-ray photon energies at resonance in XAS yields the RIXS spectrum, which is used primarily to probe the low-excited energy-loss feature which is symptomatic of the electron correlation. XAS and XES measurements of the Fe $L_{2,3}$ -edges were taken at beamlines 7.0.1 and 8.0 at the Advanced Light Source (ALS) at Lawrence Berkeley National Laboratory (LBNL). In the Fe L -edge x-ray absorption process, the electron in the Fe $2p$ core level was excited to the empty $3d$ and $4s$ states and, then, the XES spectra were recorded as the signal associated partial densities of states with Fe $4s$ as well as Fe $3d$ character. The RIXS spectra were obtained by properly selecting various excitation energies to record the XES spectra, based on the x-ray absorption spectral profile. The XAS spectra were obtained with an energy resolution of 0.2 eV by recording the sample current. Additionally, the x-ray emission spectra were recorded using a high-resolution grazing-incidence grating spectrometer with a two-dimensional multi-channel plate detector with the resolution set to 0.6 eV (Norgdren et al., 1989). Surface oxidation is of priority concern in Fe-based superconductors; to prevent oxidation of the surface, all data were gathered on a surface of the sample that was cleaved *in situ* in a vacuum with a base pressure of 2.7×10^{-9} torr.

3. Results and discussion

3.1. Microstructure of FeSe and FeTe

Figure 1 (a) shows the tetragonal crystal structure of FeSe and its building blocks, i.e. Se-Fe tetrahedra and Fe-Se pyramidal sheets. Figure 1 (b) shows the electronic energy level of the individual constituent elements and FeSe_x (indicating the hybridization band). Figure 2 shows the XRD patterns of the FeSe_x ($x=0.9$, 0.88 and 0.85) crystals, which represent the superconducting FeSe phase. The patterns are correlated with the $P4/nmm$ and indexed in the figure. Weak hexagonal reflections are also observed. According to this figure, the main diffraction peak (101) shown expanded in the inset shifts to a lower 2θ as x decreases, indicating an increase in the lattice parameters. The lattice parameters calculated from these patterns are $a=b=3.771 \text{ \AA}$, $c=5.528 \text{ \AA}$ for $x=0.9$, $a=b=3.775 \text{ \AA}$, $c=5.528 \text{ \AA}$ for $x=0.88$ and $a=b=3.777 \text{ \AA}$,

$c=5.529 \text{ \AA}$ for $x=0.85$. Experimental results indicate that the $a=b$ parameter increases incrementally as x decreases. Simultaneously, a markedly smaller change occurs in the c -parameter. Thus, the a - b plane variation surpasses that of the c axis. These lattice parameters are very close to those described in the literature for Se deficient powders (Hsu et al., 2008).

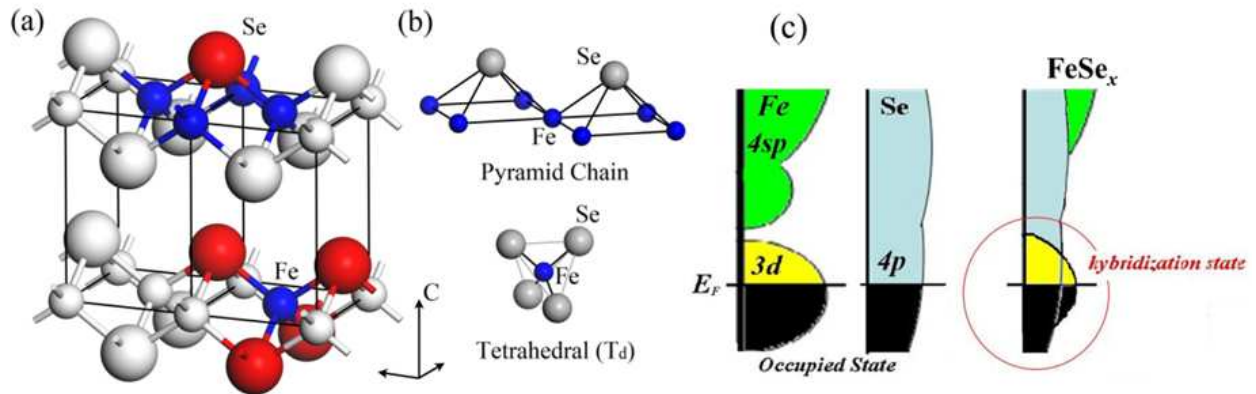


Figure 1. (a) Illustration of the crystal structure of tetragonal FeSe_x, where the blue (small balls) and red (large balls) denote Fe and Se, respectively; the pyramid chain and tetrahedral arrangements are marked in color in the unit cell. Hybridization is shown in two color bonds; (b) the local symmetry of Se atom (in pyramid chain) and Se atom (in tetrahedral geometry) shown separately; (c) energy level diagram of the FeSe_x system along with individual elements. The hybridization and unoccupied states in the FeSe are highlighted by a circle.

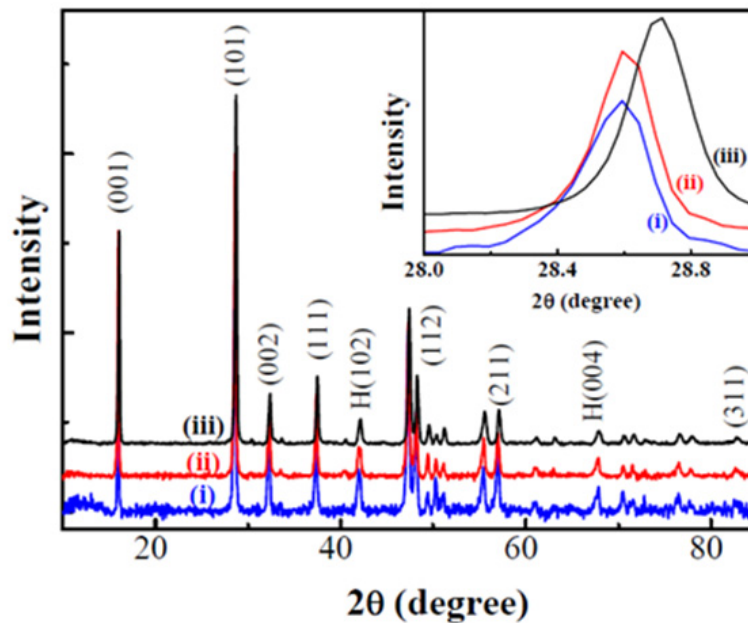


Figure 2. Powder XRD patterns of FeSe_x crystals with $x =$ (i) 0.85, (ii) 0.88 and (iii) 0.9. The patterns are fitted to the P4/nmm space group and indexed. Hexagonal phase reflections are denoted by a prefix H.

Conversely, FeTe with the same tetragonal crystal structure is stable up to a significantly higher temperature, $\sim 1200 \text{ K}$. As is expected, replacing Se atoms within FeSe with Te

stabilizes the tetragonal phase at a synthetic temperature close to or above 731 K. This observation correlates well with our X-ray diffraction analysis. This phenomenon is likely owing to that Te, which has a larger atomic size than Se, inhibits interatomic diffusion in the FeSe lattice. In contrast, Se atoms move easily in the larger FeTe lattice. The lattice parameters calculated from FeSe_{1-y}Te_y patterns are increased with a increasing y (Yeh et al., 2009; Yeh et al., 2008). Analysis results indicate that T_c and gamma angle of the distorted lattice both reach a maximum value at FeSe_{0.56}Te_{0.41} (~50% Te substituted). This correlation between the gamma angle and T_c indicates that T_c heavily depends on the level of lattice distortion and the distance of the Fe-Fe bond in the Fe-plane. Results of above studies correspond to the electron-orbital symmetry based on the XAS measurements, as discussed below.

3.2. Electronic structure results based on X-ray spectroscopy

3.2.1. FeSe_x crystals

XAS spectra of the transition metal Fe K-edge ($1s \rightarrow 4p$) in Fig. 3(a) are mostly related to the partial density of $4p$ states of the iron site (Fig. 1(c)). Unoccupied states in the $3d$ (due to quadruple transition) and $4sp$ bands are sensitive to the local structure and the type of the nearest neighbors (de Groot et al., 2009; Chang et al., 2001; Longa et al., 1999). Above spectra can therefore obtain information about the changes in the electronic states possibly originating from changes in the environment of the Fe ions such as Se vacancies in the present case. Figure 3 shows the Fe K-edge absorption spectra of FeSe_x crystals along with the standards Fe, FeO, Fe₂O₃ and Fe₃O₄. All spectra are normalized at the photon energy ~100 eV above the absorption edge at $E_0 = 7,112$ eV (the pure Fe K absorption edge energy). The spectra of the crystals appear to be close to the Fe metal foil, indicating that the crystals are free from oxidation. The recent Fe L -edge ($2p_{2/3} \rightarrow 3d$ transition) spectra measured before and after cleaving the samples in UHV further confirm this observation, as shown in the inset of Fig 3(a). The oxidation peak is observed in the crystal before cleaving but it does not appear after cleaving, indicating the possible formation of a thin oxide layer on the surface during handling. Such a thin layer may negligibly impact the deeper penetrating K-edge measurements. Since our measurements are made after cleaving the crystals under vacuum this possibility of surface oxidation is even eliminated. The following section describes in more detail the FeSe_x electronic structure of the $3d$ states obtained by XAS measurements and resonant inelastic x-ray scattering (RIXS) at the Fe $L_{2,3}$ edges. The observations agree with those of Yang *et al.* (2009) on Fe-pnictides 1111 and 122 systems, as well as those of Lee *et al.* (2008) when using first principles methods to study FeSe_x system. Therefore, our results on the oxygen free FeSe_x crystals eliminate the possibility of oxygen in superconductivity, as is case in the LaO_{1-x}F_xFeAs system.

These spectra reveal three prominent features, A₁, A₂ and A₃ (Fig. 3(a)), of which, A₁ could be assigned to the $3d$ unoccupied states originating from the Fe-Fe bonds in metallic iron. The features A₂ and A₃ refer to the unoccupied Fe $4sp$ states. The rising portion of the broad feature A₂ (~7,118.8 eV) appears as a broad peak labeled e1 at ~7,116.8 eV, which appears to be well separated in the first derivative plots of the spectra shown in Fig. 3(b). While not

observed in the spectra of the reference Fe metal foil or oxides, this broad peak is a part of the Fe $4sp$ band. The e_1 feature appears at an energy between those of the Fe metal and FeO and, therefore, originates from a different interaction, as discussed later. Based on these first derivative plots, this study also evaluates a formal charge of Fe, in conjunction with the three standards FeO (Fe^{2+}), Fe_2O_3 (Fe^{3+}) and Fe_3O_4 ($\text{Fe}^{2.66+}$). Extrapolating the energy of FeSe_{0.88} with those of the standards allows us to obtain a formal charge of $\sim 1.8+$ for Fe in these crystals, thus establishing the electronic charge of Fe in the covalency ($2+$). Our results further indicate that the peak (energy) position does not increase in energy with a decreasing x , implying that the effective charge (valence) of Fe does not change with x . This finding is consistent with the above Fe L -edge spectra as well as RIXS analysis (Tamai et al., 2010). Thus, the possible electronic configurations of Fe in the ground state can be written as $3d^{6.2}$ or $3d^6 4s^{0.2}$, indicating a mixture of monovalency ($3d^6 4s^1$ or $3d^7$) and divalency ($3d^6$).

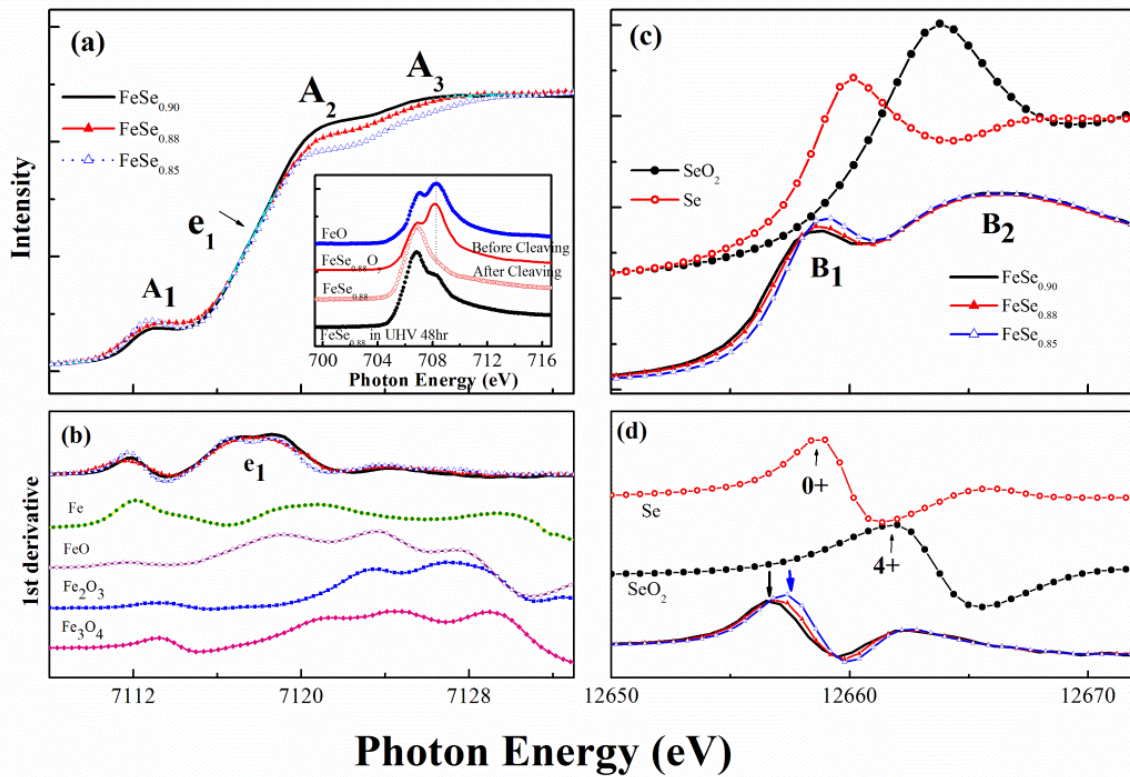


Figure 3. (a) Fe K-edge ($1s \rightarrow 4p$) absorption spectra of FeSe_x with different Se contents, and the inset shows the XAS Fe L_3 -edge spectra of $\text{FeSe}_{0.88}$ crystal before and after cleaving *in situ* in a vacuum (b) the first derivative plots of the same spectra. The spectra of the standards - Fe-metal foil, FeO, Fe_2O_3 and Fe_3O_4 are also given alongside the sample spectra. (c) The Se K-edge ($1s \rightarrow 4p$) absorption spectra FeSe_x with different Se contents, along with the standards Se metal and SeO_2 and (d) the first derivative plots of the same spectra.

Figure 3(c) shows the Se K-edge spectra of the FeSe_x crystals and Se and SeO_2 standards, while Fig. 3(d) displays the corresponding first derivative plots to highlight energy changes in the spectra. The spectra represent mainly Se character without any trace of SeO_2 , indicating the absence of oxidation, even in the deeper layers of the FeSe_x crystals. The spectra exhibit two peaks B₁ and B₂. The B₁ feature at photon energy around 12,658 eV,

formally assigned to the transitions $1s \rightarrow 4p$, increases slightly in intensity as well as shifts to a higher energy as x is decreased. This suggests an increase in the Se $4p$ unoccupied states i. e. in the upper Hubbard band (UHB). According to the first derivative plots, a formal charge of $\sim 2.2^-$ is obtained for Se in the $x=0.88$ crystal by interpolation with the energies of the standards Se and SeO_2 (as in the case of Fe). This finding agrees with a total charge of 0 when the formal charges of Fe and Se are added ($\text{Fe}^{1.8+} \text{Se}_{0.88}^{2.2-}$), thus establishing the role of the electronic charge of Se in the covalency (2-).

The excess negative charge of -0.2 found in Se can be explained as follows. The electronic charge of Fe in the covalent FeSe_x should be $2+$. However, in this work, a formal charge of $1.8+$ is obtained, implying that some electronic charge is returned to Fe due to the Se deficiency. However, the covalent charge of Se should be 2^- yet 2.2^- is obtained here, which is beyond the 6 electron occupancy of the $4p$ state orbitals. The Se K-edge spectra reveal a hole increase with a decreasing x ; however, no change in the Fe K-edge suggests a change in valence. According to the soft x-ray photoemission spectroscopy (XPS) measurements of Yamasaki *et al.* (2010), the close distance between Se and Fe may increase the covalence of the Fe-Se bond due to the hybridization of Se $4p$ and Fe $3d$ states. Yoshida *et al.* (2009) also observed an adequate correlation between their DOS calculations and the XPS spectra, which show a feature corresponding to the Fe $3d$ -Se $4p$ hybridization. Theoretical calculations of Subede *et al.* (2008) also suggest this Fe-Se hybridization. From the above discussion, we can infer that the B_1 feature (Fig. 3(c)) represents the Fe $3d$ -Se $4p$ hybridization band (Fig. 1(c)). Additionally, the increased electronic charge on Fe mentioned above is due to itinerant electrons in the Fe-Se hybridization bond and appears as a hole increase in the Se K-edge spectra. Correlating this finding with the decreasing transition width in the resistance measurements (Mok *et al.*, 2009) obviously reveals that the charge carriers responsible for superconductivity are itinerant electrons in a manner similar to the itinerant holes in the case of cuprates. Oxygen annealing in case of $\text{YBa}_2\text{Cu}_3\text{O}_{6+x}$, oxidizes Cu^{2+} to Cu^{3+} through the hybridization of Cu $3d$ -O $2p$ states. A previous study (Groni *et al.*, 1989; Merz *et al.*, 1998) assigned the Cu^{3+} state to the empty state in the Cu-O bonds, which is also referred to as the $3d^9L$ ligand state, where a hole is located in the oxygen ions surrounding a 'Cu site' (L, a ligand hole, tentatively label this as $3d^8$ -like). These itinerant holes are responsible for superconductivity. Similarly, in the case of FeSe_x , the Se deficiency is bringing about Fe $3d$ -Se $4p$ hybridization leading to itinerant electrons. According to Mizuguchi *et al.* (2008), changes in bond lengths likely result in a reduction in the width of the resistive transition due to external pressure.

Experimental results indicate that the intensity of the A_2 feature diminishes as x is decreased, indicating a lattice distortion that increases with a decreasing x . Additionally, the change in the A_2 feature is larger than that of the A_3 feature. Notably, the A_2 feature could be associated with p_{xy} (σ) and A_3 to p_z (π) orientations since multiple scattering in the XAS from p orbitals could reveal different orbital orientations, and also owing to the nature of the p orbitals, i.e. p_{xy} and p_z . We thus speculate that a larger distortion occurs in the a - b plane (Fe-Fe distance) than in the c axis. This is also seen from the XRD measurements (Fig. 2) where the change in the $a=b$ parameter is more profound than that of the c parameter (Fe-Se

distance). Therefore, the Fe orbital structure changes from $4p$ to a varying (modulating) coordination with a decreasing x . The broad feature B_2 , at ~ 20 eV above the Se K-edge appears at the same energy in the entire FeSe_x spectra, is not affected by the Se deficiency and is assigned to the multiple scattering from the symmetrical Se $4p$ states in the coordination sphere that are correlated to the local structure of the Se ions (de Groot et al., 2009). This finding correlates with the XRD results where the c parameter remains nearly unchanged. This occurrence becomes obvious when examining Fig. 1, where Se is found at the tip of the Fe-Se pyramid.

Since Se is located at the apex of the tetrahedral pyramid chain in the FeSe_x lattice (Fig. 1), removing a Se ion with a formal negative charge (-2) from the lattice would result in a Se vacancy with an effective positive charge and also repulse the surrounding positively charged Fe atoms. This finding corresponds to the distortion in the ab plane, as discussed above. Additionally, according to Lee *et al.* (2008), the Fe atoms around the vacancy may function similar to magnetic clusters.

3.2.2. Electron correlations of $\text{FeSe}_{1-y}\text{Te}_y$

As discussed above, due to the unstable phase of stoichiometry FeSe and efforts to more thoroughly understand the origin of superconductivity in this class of materials, of worthwhile interest is to investigate the effect of chemical substitution on FeSe in order to maintain or improve the superconducting property and stabilize the crystal structure. Figure 4(a) compares Fe $L_{2,3}$ -edges XAS spectra of $\text{FeSe}_{1-y}\text{Te}_y$ before and after cleavage *in situ*, in which an oxidized iron foil is used as a reference sample. Of the two XAS lines, A_1 and B_1 , at the L_3 -edge of the oxidized iron foil, B_1 are prominent from the uncleaved samples, indicating that the sample surface is seriously contaminated by oxygen. The shoulder-like line B_1 , which originates from Fe-O bonding in cleaved samples, is smeared. As is well known, iron oxide yields B_1 . However, this line is missing from the spectra of cleaved $\text{FeSe}_{1-y}\text{Te}_y$ samples, indicating that iron oxide is only a very minor constituent. This finding reflects the importance of cleavage *in situ* for making spectral measurements of samples in this class. Figure 4(b) further illustrates how sensitive the FeSe (without Te doping) is, in which it oxidizes very easily, even in an ultra-high vacuum chamber with a base pressure of $\sim 2.7 \times 10^9$ torr. The study of $\text{FeSe}_{0.88}$ crystal in an earlier section observed this phenomenon. In this work, XAS of pure FeSe is obtained, and the pure compound oxidizes within 12 hours, as indicated by a comparison with a doped sample ($\text{FeSe}_{1-y}\text{Te}_y$, $y=0.5$). The high-energy shoulder structure, as denoted by a dash line, is associated with the Fe-O bond; it is absent right after *in-situ* cleavage of either sample. This structure appears again in the FeSe sample when placed in a vacuum for 12 hr, yet does not reappear in the doped samples. This finding demonstrates that pure FeSe suffers from serious surface oxidation. Capable of enhancing the T_c value, Te doping can also stabilize the crystal structure. Figure 4(c) presents Fe $L_{2,3}$ -edges XAS spectra of $\text{FeSe}_{1-y}\text{Te}_y$, by using Fe metal, oxidized foil and Fe_2O_3 as reference samples. Unoccupied Fe $3d$ orbitals are probed using XAS. The spectra reveal two major transitions. Governed by the dipole selection rule, the transition is mainly due to

$2p^63d^6-2p^53d^7$ transition, in which an Fe $2p$ electron is excited into an empty $3d$ state. Spin-orbit splitting separates the $2p$ state into $2p_{3/2}$ and $2p_{1/2}$ states, yielding two prominent absorption features around 707 eV (L_3) and 720 eV (L_2). XAS at the transition-metal L -edge probed unoccupied $3d$ states, which are sensitive to the chemical environment, valence state, crystal field and $3d$ electronic interactions. The ratio of intensities of the two major absorption features is largely determined by the high- or low-spin ground states through the crystal-field effect. XAS of Fe_2O_3 reveals a strongly split structure at both L_2 and L_3 absorption edges, which is formed by the interplay of crystal field and electronic interactions. Fe-O does not contribute to the $\text{FeSe}_{1-y}\text{Te}_y$ spectra, and no spectral profile resembles that of Fe_2O_3 or oxidized foil. As is generally assumed, the shoulder at the high-energy tail (dotted portion) of the Fe L_3 line in the $\text{FeSe}_{1-y}\text{Te}_y$ samples is associated with covalent sp^3 bonds between Fe $3d$ and Se $4p$ /Te $5p$ states (Bondino et al., 2008). $\text{FeSe}_{1-y}\text{Te}_y$ yields no observable line splitting or change in intensity ratio, implying a weak crystal-field effect and also that the Fe ion favors a high-spin ground state. Line shapes in the spectra of these cleaved crystals in the UHV chamber resemble those of iron metal, indicating metallic nature and a localized $3d$ band (Yang et al., 2009). As is anticipated, the variation in the full width at half maximum (FWHM) of the Fe L_3 peak in the XAS and the width of the Fe $3d$ band with localized character is smaller than those of Fe because the Fe-Fe interaction is stronger (Nekrasov et al., 2008).

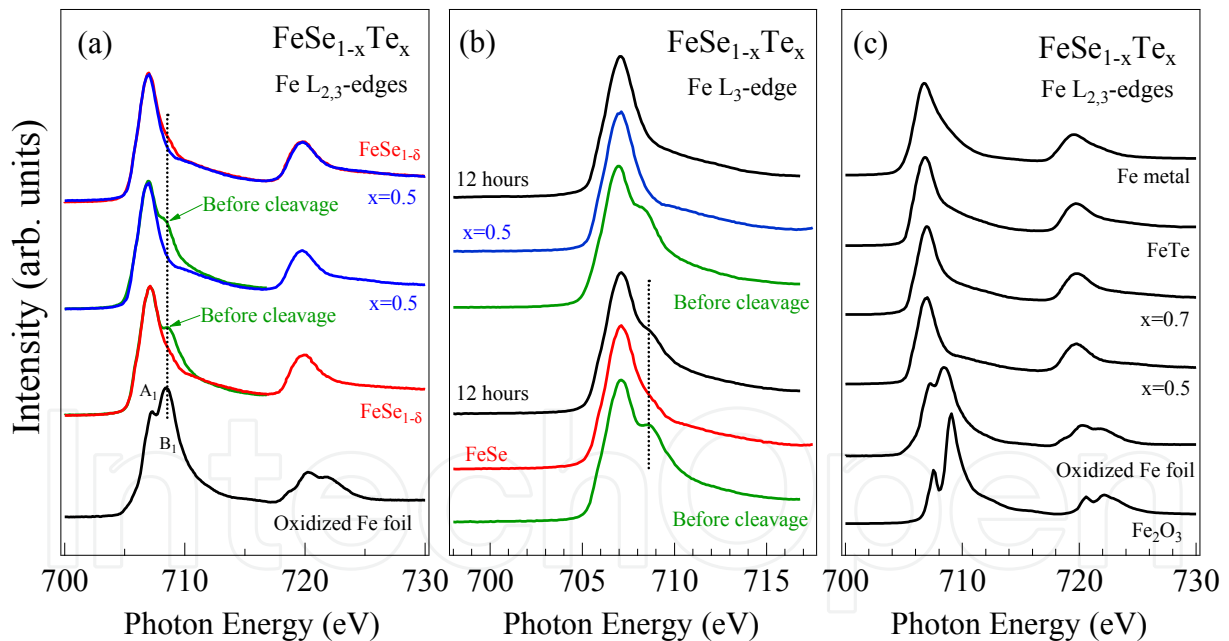


Figure 4. (a) Comparison of Fe $L_{2,3}$ -edge XAS of $\text{FeSe}_{1-y}\text{Te}_y$ before and after cleavage *in situ*, using oxidized iron foil as a reference. (b) FeSe is highly sensitive, even in the vacuum; in addition, it oxidizes within 12 hours. (c) Fe $L_{2,3}$ -edge XAS of $\text{FeSe}_{1-y}\text{Te}_y$ cleaved *in situ*. Samples of Fe metal, oxidized foil and Fe_2O_3 serve as references.

Figure 5(a) describes the RIXS (lower part) obtained at selected energies (letters a-g), as denoted by arrows in XAS (upper part). The upper RIXS spectrum is obtained at an excitation photon energy of 735 eV, far above the Fe L_3 -edge absorption threshold. This

spectrum is commonly referred to as the so-called non-resonant normal emission spectrum. This non-resonant spectrum reveals two main fluorescent features around 704 eV and 717 eV, resulting from de-excitation transitions from occupied $3d$ states to the $2p_{3/2}$ and $2p_{1/2}$ holes, respectively, which are thereby refilled. The RIXS recorded with various excitation energies, a-f, include the strong 704 eV peak, as observed in the non-resonant spectrum. At an excitation energy close to that of the L_2 absorption feature, the line at 717 eV emerges and remains at the same energy as the excitation energy increases beyond the L_2 edge. As indicated by arrows in spectra d and e, small bumps appear at energies of approximately 710 and 716 eV. These energies track well the excitation energies and, therefore, are caused by elastic scattering. As magnified in the inset, the fluorescent feature of both samples does not follow the excitation energy and well overlaps the line at 704 eV in the non-resonant spectrum. Notably, RIXS includes no energy loss feature, which is generally associated with electron correlation and excitations.

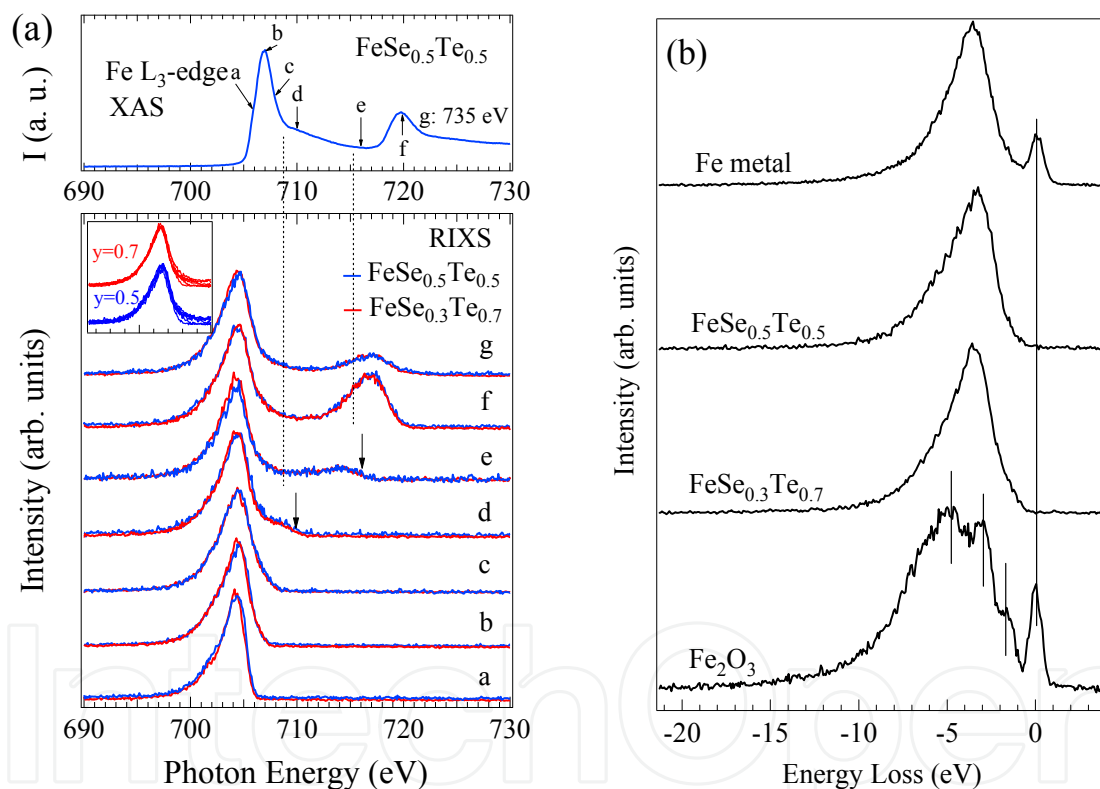


Figure 5. (a) RIXS (lower part) obtained at selected energies (a-g), as denoted by arrows in XAS (upper part). Inset shows the fluorescent feature of both samples, which overlaps well with the line at 704 eV in the non-resonant spectrum. (b) Comparison of RIXS resonantly excited at 708 eV for samples with $y=0.5$ and 0.7 and reference samples Fe_2O_3 and pure iron metal.

Figure 5(b) compares RIXS obtained with resonant excitation at 708 eV from samples with $y=0.5$ and 0.7 and from reference samples Fe_2O_3 and pure iron metal. They are displayed with an energy loss scale; elastic scattering produces the feature at an energy loss of zero. Notably, Fe_2O_3 RIXS exhibit more complex energy-loss features, which are marked by short vertical lines. These features are enhanced at particular excitation energies because of inter-

electronic transitions, and are identified as $d-d$ excitations (Duda et al., 2000). Fe metal yields one main fluorescent line and a more symmetric profile. Spectra of $\text{FeSe}_{1-y}\text{Te}_y$ are also obviously dominated by only a single line and resemble that of Fe metal, implying metallic character. Analysis results of the Coulombic interaction and Fe $3d$ bandwidth indicate the lack of excitation-induced energy-loss features in RIXS of iron-pnictide samples, implying a weak correlation in the iron-pnictide system (Yang et al., 2009). Therefore, known metallic iron and insulating iron oxide must be compared further to reveal the importance of electron correlation and metallicity.

Just as XAS demonstrates the density of unoccupied states (DOS) in d orbitals, non-resonant XES are interpreted simply as revealing the occupied DOS of d states, which is dominated by Fe $3d$ orbitals near the Fermi level. Figure 6 (a) shows the non-resonant Fe $L_{2,3}$ -XES of Fe_2O_3 , $\text{FeSe}_{1-y}\text{Te}_y$ and Fe metal. The spectra of $\text{FeSe}_{1-y}\text{Te}_y$ and Fe are nearly identical in both shape and energy, indicating that the experimental determination of the contribution of occupied Fe $3d$ states in $\text{FeSe}_{1-y}\text{Te}_y$ closely resembles that of Fe metal. The ratio of intensities of L_2 and L_3 XES should equal $1/2$ for free atoms, reflecting the statistical populations of the $2p_{1/2}$ and $2p_{3/2}$ energy levels. However, in metals, Coster-Kronig transitions markedly reduce this ratio, revealing the correlations and metallicity of a system (Raghu et al., 2008). Figure 3(b) presents ratio I_2/I_3 , i.e. the ratio of integrated intensities of the XES L_2 and L_3 lines. $\text{FeSe}_{1-y}\text{Te}_y$ samples with $y=0.5$ and $y=0.7$ have almost identical I_2/I_3 intensity ratios. These ratios are closer to that of correlated Fe_2O_3 than to that of the metal, indicating that the character of $\text{FeSe}_{1-y}\text{Te}_y$ more closely resembles that of correlated Fe_2O_3 . This finding corresponds to that of the Fe $3d$ states in $\text{FeSe}_{1-y}\text{Te}_y$ systems, which exhibit more localized than itinerant character, as denoted by a smaller FWHM in XAS than that of Fe-pnictides.

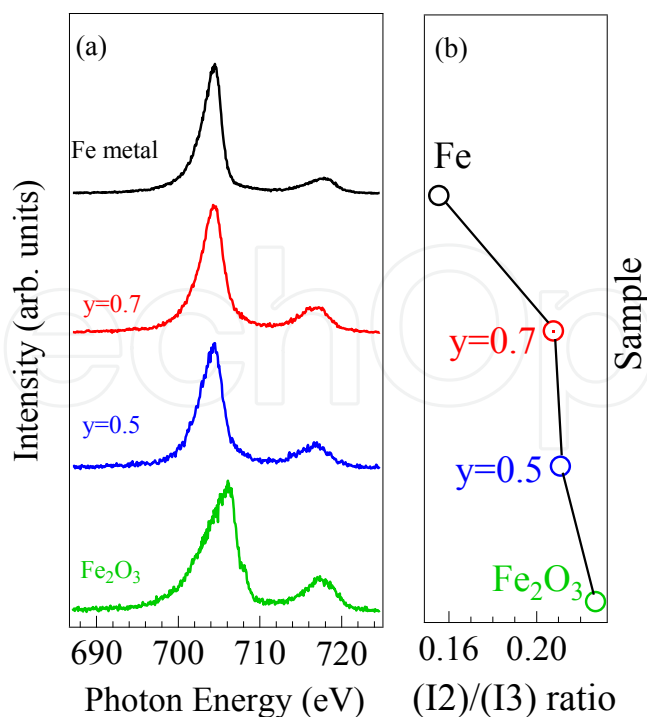


Figure 6. (a) Comparison of non-resonant Fe $L_{2,3}$ -XES of Fe_2O_3 , $\text{FeSe}_{1-y}\text{Te}_y$ and Fe metal. (b) Ratio of integrated intensities (I_2/I_3) of XES L_2 and L_3 lines.

The similarity between XAS and XES of $\text{FeSe}_{1-y}\text{Te}_y$ and those of Fe metal signifies the importance of metallicity in this system. This metallicity is further and directly ascertained from absorption-emission spectra, which, with a carefully calibrated energy scale, can reveal both the occupied and the unoccupied electronic densities of states around the Fermi level. Figure 7(a) displays the absorption-emission spectra, revealing the DOS of Fe $3d$ states across the Fermi level. An arrow indicates the intersection of XAS and XES, indicating that $\text{FeSe}_{1-y}\text{Te}_y$ can be regarded as metallic in nature. Figure 7(b) shows the overlain spectra of $\text{FeSe}_{1-y}\text{Te}_y$ and Fe. The Fe spectrum has a single line, which is narrower than the corresponding line of $\text{FeSe}_{1-y}\text{Te}_y$. This dominant line in the spectrum of $\text{FeSe}_{1-y}\text{Te}_y$ is slightly broader than that of Fe, perhaps owing to Se hybridization state in the lower-energy region (Yamasaki et al., 2010; Subede et al., 2008).

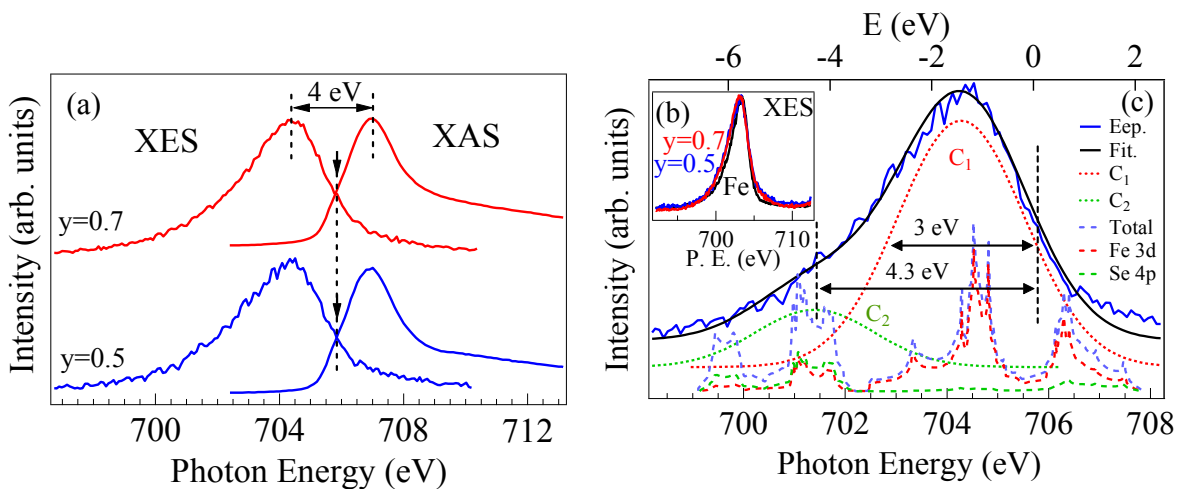


Figure 7. (a) Absorption-emission spectrum of $\text{FeSe}_{1-y}\text{Te}_y$ ($y=0.5$ and 0.7). Intersection yields denotes E_F . (b) Spectra of $\text{FeSe}_{1-y}\text{Te}_y$ ($y=0.5$ and 0.7) and Fe metal. A deviation originates from Fe-Se hybridized states. (c) Fe L_3 -XES line is fitted by two components (dotted lines). The dashed lines refer to calculated DOS (from Subede et al., 2008).

Iron pnictides are weakly correlated systems, unlike high- T_c cuprates. However, a theoretical work has established that Fe-Se may not be correlated as weakly as Fe pnictides (Aichhorn et al., 2010). An important question that arises concerns whether compounds in the FeSe family exhibit a weak correlation, like that of iron pnictides, or a strong correlation, similar to that in high- T_c cuprates. Therefore, information concerning bandwidth of the Fe $3d$ states must be obtained from spectral results. An estimate of the FWHM in $\text{FeSe}_{1-y}\text{Te}_y$ XES yields a width of 4.1 eV. This value reflects the fact that core-hole lifetime and multiplet broadening, and are not associated with the Fe $3d$ bandwidth. Figure 7 (c) displays a deconvoluted spectrum that includes a single dominant line (C_1) and a low-energy contribution (C_2), which is consistent with published x-ray data (Freelon et al., 2010). The main line is associated primarily with Fe $3d$ bands; in addition, the contribution in the low-energy region is interpreted as originating from the hybridization of Fe $3d$ and Se $4p$ states (Kurmaev et al., 2009). The low-energy shoulder originates from hybridization of Fe $3d$ and As $4p$ states in the FeAsFO "1111" system. Analytical results

indicate that the FeSe "11" system is simpler than the "1111" system: the low-energy contribution therefore originates from hybridization of Fe $3d$ -Se $4p$ without calculation forecasts. This hybridization of Fe $3d$ -Se $4p$ is also consistent with recent density functional calculations (Subede et al., 2008). According to the projected density of states (adopted from Subede et al., (2008)) in the bottom of Fig. 7(c), peak C_1 is mainly due to the Fe $3d$ states. Peak C_2 lies far below the Fermi level, and can be ascribed to the hybridized Fe $3d$ -Se $4p$ states. Width of the dominant peak in Fe L_3 XES is ~ 3 eV. Given the instrumentation resolution, this value is taken as a guide for an upper limit of the Fe $3d$ bandwidth. Estimation results of ~ 3 eV for the Fe $3d$ bandwidth correlate with the on-off-resonance photoemission results, revealing that Fe dominates the binding energy range of 0-3 eV (Yamasaki et al., 2010). The low-energy contribution at 4.3 eV below E_F is attributed to Se $4p$ states, which corresponds to the on-off-resonance photoemission results (Yamasaki et al., 2010) and DOS calculation (Subede et al., 2008). The degree of electron correlation implies the relative magnitudes of the Coulomb interaction U and bandwidth W . Additionally, U is simply taken as the energy difference between the occupied and unoccupied states near E_F , and is estimated to be ~ 4 eV. This value matches values presented in another work, in which U of the FeSe system has been predicted to be ~ 4 eV (Aichhorn et al., 2010). The values imply that the magnitude of U is larger than that of the upper limit of the estimated Fe $3d$ bandwidth. The result $U/W > 1$ in this work reflects a strong electronic correlation due to competition between the localized effect of U and the itinerant character of W (Zaanen et al., 1985).

Various experiments and theoretical calculations have been undertaken, especially for the "1111" and "122" systems, to elucidate electron correlation in these Fe-based compounds. Now, the results herein concerning the "11" system are compared with those obtained elsewhere for "1111" and "122" compounds. Comparing the photoemission spectrum (PES) of Fe with the Cu $2p$ core-level spectra of CeFeAsO_{0.89}F_{0.11} (1111) (Bondino et al., 2008) and high- T_c cuprates (La_{2-x}Sr_xCuO₄ and Nd_{2-x}Ce_xCuO_{4- δ}) (Steeneken et al., 2003) reveals the absence of satellite structures with higher binding energies in the Fe $2p$ spectra. This finding implies the presence of strongly itinerant Fe $3d$ electrons, which contrasts with the observation from the Cu $2p$ spectra in high- T_c cuprate. Further comparing the Fe L_3 XAS spectra reveals the lack of a well-defined multiplet structure, which is indicative of the delocalization of $3d$ band states, and subsequently providing complementary evidence of the itinerant character of Fe $3d$ electrons. Strongly itinerant $3d$ electrons are thus an important characteristic of the Fe-based superconductor, implying that it does not exhibit as strong correlations as a high- T_c cuprate. A previous study has examined the extent of electron correlations in PrFeAsO by using coupled x-ray absorption and emission spectroscopy (Freelon et al., 2010). From the spectroscopic results herein, the bandwidth of the Fe $3d$ states is estimated to be ~ 2 eV, which is similar to or larger than the theoretical Coulomb parameter $U \leq 2$ eV. The relative magnitudes of U and W thus simply suggest that the "1111" system exhibits weak to intermediate electron correlations (Freelon et al., 2010). A detailed study involving the theoretical calculations for both "1111" and "122" Fe-pnictides was performed, with its results correlating well with experimental x-ray

spectroscopic results (Yang et al., 2009). A cluster calculation was performed to highlight the role of strong Coulomb correlations; spectral features associated with strong correlations are shown in the theoretical results, yet are suppressed in the experimental data. Based on a direct comparison of the energy position of this feature in the experimental data and that in the cluster simulation, an upper limit of the Hubbard U of 2 eV is determined; this value is markedly smaller than the Fe $3d$ bandwidth. This finding suggests that Fe-pnictides should be viewed as a weakly correlated system. Although the XAS results herein resemble those in previous studies for Fe-pnictides and do not show the well-defined multiplet structure that is exhibited by Fe ionic oxides, two important differences are observed upon closer inspection: (a) the high-energy shoulder intensity of $\text{FeSe}_{1-y}\text{Te}_y$ is lower than that of Fe-pnictides, and (b) the linewidth of the main peak in the XAS spectrum of Fe metal is smaller than that of Fe-pnictides (Yang et al., 2009). The weak and broad shoulder is owing to hybridization of Fe $3d$ - Z np states (Z : sp element). Thus, this reduction in intensity implies less hybridization than exhibited by other Fe-based "1111" and "122" systems. This finding is consistent with the observation that the linewidth of the Fe $3d$ main peak from FeSe is narrower than those from the "1111" and "122" systems. The presence of localized Fe $3d$ electrons in the FeSe system is also confirmed by XES, which can extract information about the bandwidth of the Fe $3d$ states. As is estimated, the bandwidth in this work is ~ 3 eV, although this value is larger than that, ~ 2 eV, found in a previous study of the "1111" system (Bondino et al., 2008). However, according to our spectroscopic results, the Coulomb parameter U is estimated to be ~ 4 eV, which exceeds values reported elsewhere, which range from 0.8 eV to 2 eV (Yang et al., 2009; Bondino et al., 2008; Nekrasov et al., 2008). Recent calculation studies also support the Coulomb parameter $U \sim 4$ eV in this work. Above differences suggest that the FeSe system differs from "1111" and "122" compounds, and the FeSe "11" system is probably not a weakly correlated system.

The electronic properties discussed above concern Fe $3d$ orbitals. The correlation between the superconducting behavior and the band structures, as well as interaction of the d - d and d - p states, may also play a vital role in these systems, as revealed by the XANES tests on FeSe_x single crystals at section 3.3.1. As mentioned earlier, although doping of Te ($y=0.5$) enhances the T_c value, under- or over-doping decreases this value. Origin of the enhancement must be clarified. The Fe K-edge spectral profiles of the $\text{FeSe}_{1-y}\text{Te}_y$ are identical and appear to remain unaffected by Te doping (Fig. 8), which is consistent with observations of Fe L -edge XAS and RIXS. This finding suggests that the valence state and the electronic structure around the iron sites resemble each other. Additionally, the electronic configuration depends heavily on the hybridization between the orbitals of the Fe ($3d$) – Se($4p$)/Te($5p$) states. Accordingly, the electronic properties of $4p(5p)$ -character, which are identified from the Se (Te) K-edge XAS spectra, must be further examined. Figures 9 (a) and 9 (b) display the Se and Te K-edge spectra, respectively. The insets highlight the energy shifts in these spectra. Se K-edge spectra have a spectral line shape resembling that in FeSe_x series. The spectra are explained by a projection to the local electronic transition from the Se inner $1s$ to the outer $4p$ state. The spectra reveal two peaks, A_2 and B_2 . Peak A_2 at a photon energy of around 12,658 eV originates from Fe-Se hybridized states. The peak of the doped sample has an increased intensity and shifts to a higher energy. According to related

investigations (Joseph et al, 2010), the increase in peak A₂ intensity is owing to an increase in the strength of Fe 3d-Se 4p hybridization. The upward shift in energy is the result of an increase in the valence states. The measured energies of the absorption edge follow the order of increasing photon energy $y=0.3$, 0.7 and 0.5, as displayed in the inset. Figure 10 plots those values. Notably, the position of the absorption edge is related to the valence state; the valence state is highest at $y=0.5$, implying that the carriers between Fe and Se are itinerant electrons in the Fe-Se hybridization band, causing a valence change upon Te substitution. This increase in the valence is an indication of the change in coordination geometry and the increase in the number of 4p holes. The spectra thus provide evidence that the 4p holes are increased the most upon Te substitution when $y=0.5$. The change in the number of holes that is caused by the variation in the strength of the Fe 3d-Se 4p hybridization band is also confirmed in the x-ray absorption study of the Se deficiencies in the FeSe_x system. Additionally, the number of holes changes with the superconductivity (Fig. 10) in a manner resembling that in cuprate, whose itinerant holes, via the hybridization of Cu 3d-O 2p states, are responsible for superconductivity. Consequently, the change in valence implies a change in the number of holes by Fe 3d-Se 4p hybridization, subsequently forming itinerant holes, as occurs in Se-deficient FeSe. Notably, the broad feature B₂ appears around 20 eV above the absorption threshold in all spectra. According to the earlier discussion of section 3.2.1 and Joseph *et al.*, (2010) this feature is attributed to multiple scatterings from symmetrical Se 4p states in the coordination sphere, which is related to the local structure of the Se site. This broad feature appears at the same energy in all of the FeSe_x spectra and remains unaffected by the Se deficiency. This finding implies similar multiple scattering from Se 4p states and the same local structure around Se ions.

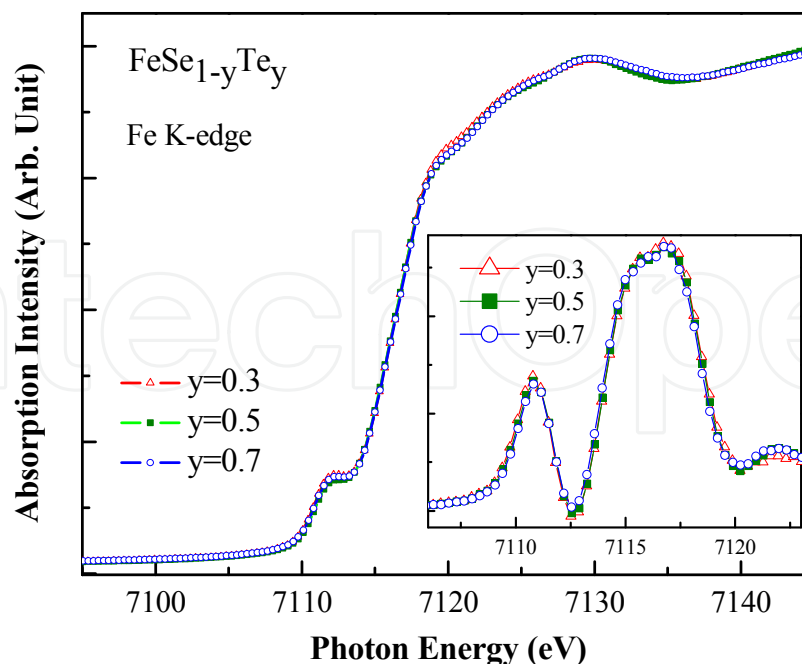


Figure 8. Fe K-edge XAS spectral profiles of FeSe_{1-y}Te_y are identical and appear to remain unaffected by Te doping. Insets show details of 1st differential spectra, which suggest a similar electronic state around Fe site.

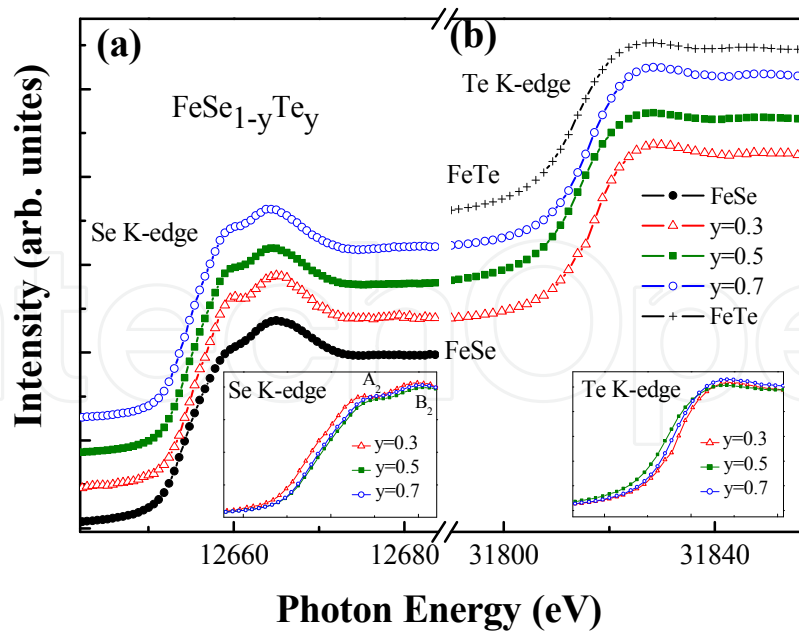


Figure 9. XAS of (a) Se K-edge and (b) Te K-edge. Insets show details of energy shifts of (a) Se K and (b) Te K-edge upon Te doping.

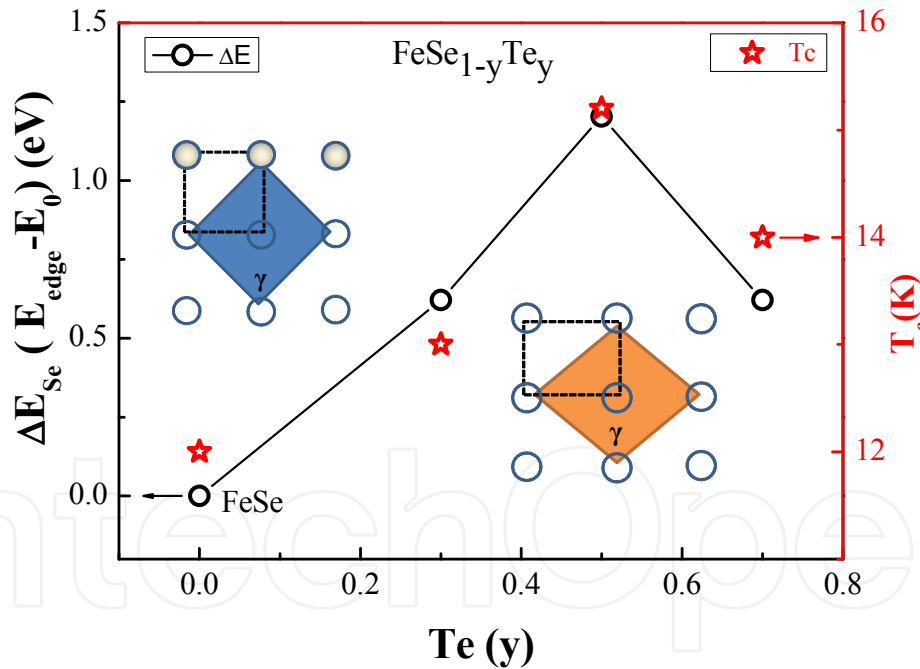


Figure 10. Energy shift of Se K-edge (black circle) and T_c as functions of Te doping. Sketch of variation of angle also shown.

However, this broad feature does not appear at the energy at which it occurred in the work of Joseph *et al.*, (2010) because of the change in the local geometry around the Se site upon Te substitution. This finding suggests local inhomogeneity, which correlates with the local inhomogeneity that was evident in XANES and EXAFS studies (Joseph *et al.*, 2010). EXAFS analysis results indicate that the Fe-Se and Fe-Te bond lengths in $\text{FeSe}_{0.5}\text{Te}_{0.5}$ differ from each

other, revealing a distinct site occupation and local in-homogeneity. A detailed polarization study of the Se K-edge demonstrates changes in the A_2 and B_2 peaks with the xy and z characteristic of the p states (Joseph et al., 2010). Owing to the natural characteristic of the p orbitals, the multiple scattering in the XAS results that are associated with p orbital symmetry reveals their different orbital orientations, thus reflecting p_{xy} and p_z character. This feature shifts to a lower energy owing to local inhomogeneity caused by doping. This finding is supported by the work of Joseph *et al.*, (2010) and implies distortion of the tetrahedral symmetry at the Se sites. Te K-edge spectra in Fig. 9 (b) include one edge feature that is associated with $1s$ to $5p$ transitions in the coordination sphere, which reflect the local envelopment of the Te ions. The inset in Fig. 9 (b) describes details of the absorption edge. The photon energy associated with the chemical shifts increases in the order $y=0.5, 0.7$ and 0.3 , i.e. a trend which contradicts the Se K-edge observations. The $y=0.5$ substitution exhibits the lowest valence state, a finding which contrasts with the Se K-edge results, possibly owing to that the charge is gained in the $5p$ orbital at the Te site. The critical and corresponding energy shift in the Se and Te K-edge features upon Te substitution is consequently indicative of an increase in the $4p$ holes and a decrease in the $5p$ holes at $y=0.5$. The tetragonal phase of FeSe has a planar sub-lattice layered structure with Se ions at the tips of the pyramid chain and an Fe plane between Se ions. The substituted Te has an ionic radius which exceeds that of Se, subsequently increasing the hybridization of Fe $3d$ -Se $4p$ /Te $5p$. Comparing Se and Te K-edges reveals an expected charge transfer between Se and Te: as Te is doped into tetragonal FeSe crystals, the number of $4p$ holes is increased by Fe $3d$ -Se $4p$ /Te $5p$ hybridization. These results are consistent with an earlier study of the structural distortion that is associated with variation in the angle γ and electron-transport properties (Yeh et al., 2008). Importantly, the change in the number of p holes between Fe-Se and Fe-Te may determine superconducting behavior.

Te doping causes structural distortions in FeSe, as revealed by detailed x-ray refinement (Yeh et al., 2008). Doping expands the lattice because the ionic radius of Te exceeds that of Se. As the doping concentration increases, angle γ varies, subsequently increasing the bond length along the c -axis and altering the density of states at the Fermi level (Yeh et al., 2008), which corresponds to density-functional calculations (Subede et al., 2008). T_c and angle γ display a similar trend: both reach their maxima at $y=0.5$. Figure 6 plots T_c against Te doping (T_c is denoted by a red star); a simple sketch of the varying γ angle is also shown. Since the electronic structure around the Fe site in $\text{FeSe}_{1-y}\text{Te}_y$ does not significantly change, exactly how Se $4p$ holes affect superconductivity should be examined. Either the energy shift or the area under the absorption feature of XAS yields the hole concentration. Therefore, in this study, the energy shift with respect to pure FeSe is determined from the Se K-edge of $\text{FeSe}_{1-y}\text{Te}_y$ and is presented in Fig. 10 as a black circle. Evolution of the edge shift reasonably estimates the hole concentration. Variation in the number of Se $4p$ holes is closely related to the change in transition temperature. The correlation between the Se $4p$ hole concentration and T_c suggests that T_c depends more heavily on the variation in the number of $4p$ holes than on the Fe-Fe interaction in the Fe plane, a claim which is consistent with the absence of

a significant change in the Fe XAS and RIXS. This finding is also consistent with the asymmetric expansion of the tetragonal lattice in relation to the structure of $\text{FeSe}_{0.5}\text{Te}_{0.5}$ – by 8 % along the c -axis, but only about 0.6% along the a -axis (Yeh et al., 2008); the Fe-Fe interaction in the Fe plane has negligible impact herein. Conversely, the role of the ligand holes and the subsequent effect of charge transfer are important. These effects may originate from Fe acting as a superexchange medium, which does not observably change from the perspective of the Fe site, a finding which is consistent with previous studies (Fang et al., 2008; Yildirim et al., 2008; Si et al., 2008). This finding may provide an important foundation for understanding the origin of superconductivity in the family of compounds considered in this study.

4. Conclusion

This study elucidates the electronic properties related to the electron correlation and superconductivity of FeSe_x and $\text{FeSe}_{1-y}\text{Te}_y$, with reference to measurements of XAS and RIXS. Spectroscopic data exhibit the signature of Fe 3d localization and different hybridization effects from those of "1111" and "122" systems. The charge balance considerations from p -hole also result in itinerant electrons. Fluctuation in the number of ligand 4p holes may arise from the charge transfer between Se and Te in the $\text{FeSe}_{1-y}\text{Te}_y$ crystals. Analysis results indicate that the superconductivity in Fe-based compounds of this class is strongly associated with the ligand 4p hole state. Additionally, the variation of T_c correlates well with the structural deformation and the change in the Se 4p holes. Moreover, the symmetry of Fe in the ab plane changes from the 4p orbital to modulating (varying) coordination geometry. XRD measurements indicate that this lattice distortion that increases with Se deficiency and the Te doped. Tetragonal FeSe with a PbO structure not only has the same planar sub-lattice as layered Fe-based quaternary oxypnictides, but also exhibits a structural stability upon Te substitution; it is a promising candidate for determining the origin of T_c in Fe-based superconductors. A fundamental question concerning the role of Fe magnetism in these superconductors is yet to be answered. The importance of charge transfer and the ligand 4p hole state should be considered as well.

Author details

Chi Liang Chen and Chung-Li Dong

Institute of Physics, Academia Sinica, Nankang, Taipei,

National Synchrotron Radiation Research Center (NSRRC), Hsinchu, Taiwan

Acknowledgement

The authors would like to thank the National Science Council of the Republic of China, Taiwan (Contract Nos. NSC-98-2112-M-213-006-MY3 and NSC-099-2112-M-001-036-MY3) for financially supporting this research. M. K. Wu, Y. Y. Chen, S. M. D. Rao, and K. W. Yeh at Academia Sinica are appreciated for providing study samples and their valuable

discussions. J.-F. Lee, T. S. Chan, C. W. Pao, J. M. Chen, and J. M. Lee of NSRRC are commended for their valuable discussions and experimental support. J.-H. Guo and W. L. Yang of Advanced Light Source are gratefully acknowledged for their experimental support.

5. References

- Aichhorn, M., Biermann, S., Miyake, T., Georges A. & Imada, M. (2010). Theoretical evidence for strong correlations and incoherent metallic state in FeSe. *Physical Review B*, 82: 064504.
- Aichhorn, M., Pourovskii, L., Vildosola, V., Ferrero, M., Parcollet, O., Miyake, T., Georges, A. & Biermann, S. (2009). Dynamical mean-field theory within an augmented plane-wave framework: Assessing electronic correlations in the iron pnictide LaFeAsO. *Physical Review B*, 80:085101.
- Arčon, D., Jeglič, P., Zorko, A., Potočnik, A., Ganin, A.Y., Takabayashi, Y., Rosseinsky, M.J. & Prassides, K. (2010). Coexistence of localized and itinerant electronic states in the multiband iron-based superconductor FeSe_{0.42}Te_{0.58}. *Physical Review B*, 82:140508(R)
- Bondino, F., Magnano, E., Malvestuto, M., Parmigiani, F., McGuire, M.A., Sefat, A.S., Sales, B.C., Jin, R., Mandrus, D., Plummer, E.W., Singh, D.J. & Mannella, N. (2008). Evidence for strong itinerant spin fluctuations in the normal state of CeFeAsO_{0.89}F_{0.11} iron-oxypnictide superconductors, *Physical Review Letters*, 101: 267001-267004.
- Chang, C.L., Chen, C.L., Dong, C.L., Chern, G., Lee, J.-F., & Jang, L.Y. (2001). X-ray absorption near edge structure studies of Fe_{1-x}Ni_xO_y thin films *Journal of Electron Spectroscopy and Related Phenomena*, 114-116:545-548.
- Cruz, C. de la, Huang, Q., Lynn, J.W., Li, Ratcliff II, J.W., Zarestky, J.L., Mook, H.A., Chen, G.F., Luo, J.L., Wang, N.L. & Dai, P. (2008). Magnetic order close to superconductivity in the iron-based layered LaO_{1-x}F_xFeAs systems. *Nature (London)*, 453:899-902.
- de Groot, F., Vankó, G. & Glatzel, P., (2009). The 1s x-ray absorption pre-edge structures in transition metal oxides. *Journal of physics: Condensed Matter*, 21: 104207.
- Dong, J., Zhang, H.J., Xu, G., Li, Z., Li, G., Hu, W.Z., Wu, D., Chen, G.F., Dai, X., Luo, J.L., Fang, Z. & Wang, N.L. (2008). Competing orders and spin-density-wave instability in La(O_{1-x}F_x)FeAs. *Europhysics Letters*, 83:27006.
- Duda, L.C., Nordgren, J., Dräger, G., Bocharov, S. & Kirchner, T. (2000). Minimal two-band model of the superconducting iron oxypnictides, *Journal of Electron Spectroscopy and Related Phenomena*, 110: 275-285.
- Fang, M.H., Pham, H.M., Qian, B., Liu, T.J., Vehstedt, E.K., Spinu, L. & Mao, Z.Q. (2008). Superconductivity close to magnetic instability in Fe(Se_{1-x}Te_x)_{0.82}, *Physical Review B*, 78: 224503-224507.
- Freelon, B., Liu, Y.S., Rotundu, C.R., Wilson, S.D., Guo, J, Chen, J.L., Yang, W.L., Chang, C.L., Glans.P.A., Shirage, P., Iyo, A.& Brigeneau, R.J. (2010). X-ray absorption and emission spectroscopy study of the effect of doping on the low energy electronic structure of PrFeAsO_{1-δ}, *Journal of the Physical Society of Japan*, 79: 074716-1-074716-7.

- Grioni, M., Goedkoop, J.B., Schoorl, R., de Groot, F.M.F., Fuggle, J.C., Schäfers, F., Koch, E.E., Rossi, G., Esteva, J.-M. & Karnatak, R.C. (1989). Studies of copper valence states with Cu L₃ x-ray-absorption spectroscopy, *Physical Review B*, 39: 1541-1545.
- Hsu, F.C., Luo, J.Y., Yeh, K.W., Chen, T. K., Huang, T.W., Wu, P.M., Lee, Y.C., Huang, Y. L., Chu, Y.Y., Yan, D.C. & Wu, M.K. (2008). Superconductivity in the PbO-type structure α -FeSe. *Proceedings of the National Academy of Sciences (PNAS)*, 105:14262-14264.
- Joseph, B., Iadecola, A., Puri, A., Simonelli, L., Mizuguchi, Y., Takano, Y. & Saini, N.L. (2010). Evidence of local structural inhomogeneity in FeSe_{1-x}Te_x from extend x-ray absorption fine structure, *Physical Review B*, 82: 020502- 020505(R).
- Joseph, B., Iadecola, A., Simonelli, L., Mizuguchi, Y., Takano, Y., T. Mizokawa, T. & Saini, N.L. (2010). A study of the electronic structure of FeSe_{1-x}Te_x chalcogenides by Fe and Se K-edge x-ray absorption near edge structure measurements, *Journal of Physics: Condensed Mater*, 22: 485702485706.
- Kamihara, Y., Watanabe, T., Hirano, M. & Hosono, H. (2008). Iron-Based Layered Superconductor La[O_{1-x}F_x]FeAs (x=0.05–0.12) with T_c = 26 K. *Journal of The American Chemical Society*, 130:3296-3297.
- Kroll, T., Bonhommeau, S., Kachel, T., Dürr, H.A., Werner, J., Behr, G., Koitzsch, A., Hübel, R., Leger, S., Schönfelder, R., Ariffin, A.K., Manzke, R., de Groot, F.M.F., Fink, J., Eschrig, H., Büchner, B. & Knupfer, M. (2008). Electronic structure of LaFeAsO_{1-x}F_x from x-ray absorption spectroscopy. *Physical Review B*, 78:220502.
- Kurmaev, E.V., McLeod, J.A., Buling, A., Skorikov, N.A., Moewes, A., Neumann, M., Korotin, M.A., Izyumov, Y.A., Ni, N. & Candfield. P.C. (2009). Contribution of Fe 3d states to the Fermi level of CaFe₂As₂, *Physical Review B* Vol. 80: 054508-054513.
- Lee, K.-W., Pardo, V. & Pickett, W.E. (2008). Magnetism driven by anion vacancies in superconducting α -FeSe_{1-x}, *Physical Review B*, 78: 174502-174506.
- Longa, S.D., Arcovito, A., Vallone, B., Castellano, A.C., Kahn, R., Vicat, J., Soldo, Y. & Hazemann, J.L. (1999). Polarized X-ray absorption spectroscopy of the low-temperature photoproduct of carbonmonoxy-myoglobin, *Journal of Synchrotron Radiation*, 6: 1138-1147.
- Lytle, F. W., Gregor, R.B., Sandstrom, D.R., Marques, E.C., Wong, J., Spiro, C.L., Huffman, G.P. & Huggins, F. E. (1984). Measurement of soft x-ray absorption spectra with a fluorescent ion chamber detector. *Nuclear Instruments and Methods in Physics Research Section A: Accelerators, Spectrometers, Detectors and Associated Equipment*, 226:542-548.
- Ma, F., Ji, W., Hu, J., Lu, Z.Y. & Xiang, T. (2009). First-Principles Calculations of the Electronic Structure of Tetragonal α -FeTe and α -FeSe Crystals: Evidence for a Bicollinear Antiferromagnetic Order. *Physical Review Letters*, 102:177003
- Malaeb, W., Yoshida, T., Kataoka, T., Atsushi, Fujimori, A., Kubota, M., Ono, K., Usui, H., Kuroki, K., Arita, R. & Hosono, H. (2008). Electronic Structure and Electron Correlation in LaFeAsO_{1-x}F_x and LaFePO_{1-x}F_x. *Journal of the Physical Society of Japan*, 77:093714.

- McQueen, T.M., Huang, Q., Ksenofontov, V., Felser, C., Xu, Q., Zandbergen, H., Hor, Y.S., Allred, J., Williams, A.J., Qu, D., Checkelsky, J., Ong, N.P. & Cava, R.J. (2009). Extreme sensitivity of superconductivity to stoichiometry in $\text{Fe}_{1+\delta}\text{Se}$. *Physical Review B*, 79:014522.
- Merz, M., Nücker, N., Schweiss, P., Schuppler, S., Chen, C.T., Chakarian, V., Freeland, J., Idzerda, Y.U., Kläser M., Müller-Vogt, G. & Wolf, Th. (1998). Site-specific x-ray absorption spectroscopy of $\text{Y}_{1-x}\text{Ca}_x\text{Ba}_2\text{Cu}_3\text{O}_{7-y}$: Overdoping and role of apical oxygen for high temperature superconductivity, *Physical Review Letters*, 80: 5192-5195.
- Mizuguchi, Y., Tomioka, F., Tsuda, S., Yamaguchi, T. & Takano, Y. (2008). Superconductivity at 27 K in tetragonal FeSe under high pressure, *Applied Physics Letter*, 93: 152505-152507.
- Mok, B.H., Rao, S.M., Ling, M.C, Wang, K.J., Ke, C.T., Wu, P.M., Chen, C.L., Hsu, F.C., Huang, T.W., Luo, J.Y., Yan, D.C., Yeh, K.W., Wu, T.B., Chang, A.M. & Wu, M.K. (2009). Growth and Investigation of Crystals of the New Superconductor $\alpha\text{-FeSe}$ from KCl Solutions. *Crystal Growth and Design*, 9(7): 3260-3264.
- Nakayama, K., Sato, T., Richard, P., Kawahara, T., Sekiba, Y., Qian, T., Chen, G.F., Luo, J.L., Wang, N.L., Ding, H. & Takahashi, T. (2010). Angle-Resolved Photoemission Spectroscopy of the Iron-Chalcogenide Superconductor $\text{Fe}_{1.03}\text{Te}_{0.7}\text{Se}_{0.3}$: Strong Coupling Behavior and the Universality of Interband Scattering. *Physical Review Letters*, 105:197001.
- Nekrasov, I.A., Pchelkina, Z.V. & Sadovskii, M.V. (2008). Electronic structure of prototype AFe_2As_2 and ReOFeAs high-temperature superconductors: A comparison, *JETP Letters*, 88: 144-149.
- Norgdren, J., Bray, G., Cramm, S., Nyholm, R., Rubensson, J.E. & Wassdahl, N. (1989). Soft x-ray emission spectroscopy using monochromatized synchrotron radiation (invited). *Review of Scientific Instruments*. 60:1690.
- Pourret, A., Malone, L. Antunes, A. B., Yadav, C.S., Paulose, P.L., Fauque, B. & Behnia, K. (2010). Strong correlation and low carrier density in $\text{Fe}_{1+y}\text{Te}_{0.6}\text{Se}_{0.4}$ as seen from its thermoelectric response. *Physical Review B*, 83:020504.
- Raghu, S., Qi, X.L., Liu, C.X., Scalapino, D.J. & Zhang, S.C. (2008). Minimal two-band model of the superconducting iron oxypnictides, *Physical Review B*, 77: 220503-220506 (R).
- Ren, Z.-A., Lu, W., Yang, J., Yi W., Shen X.-L., Li Z.-C., Che G.-C., Dong X.-L., Sun L.-L., and Zhou F., Zhao Z.-X (2008), Superconductivity at 55 K in iron-based F-doped layered quaternary compound $\text{Sm}[\text{O}_{1-x}\text{F}_x]\text{FeAs}$. *Chinese Physics Letters*, 25:2215-2216.
- Sales, B.C., Sefat, A.S., McGuire, M.A., Jin, R.Y., Mandrus, D. & Mozharivskyj, Y. (2009). Bulk superconductivity at 14 K in single crystals of $\text{Fe}_{1+y}\text{Te}_x\text{Se}_{1-x}$. *Physical Review B*, 79, 094521.
- Si, Q. & Abrahams, E. (2008). Strong correlations and magnetic frustration in the high T_c iron pnictides, *Physical Review Letters*, 101: 076401-076404.
- Steeneken, P.G., Tjeng, L.H., Sawatzky, G.A., Tanaka, A., Tjernberg, O., Ghiringhelli, G., Brookes, N.N., Nugroho, A.A. & Menovsky A.A. (2003). Crossing the gap from p- to n-

- type doping: nature of the states near the chemical potential in $\text{La}_{2-x}\text{Sr}_x\text{CuO}_4$ and $\text{Nd}_{2-x}\text{Ce}_x\text{CuO}_{4.8}$, *Physical Review Letters* Vol. 90: 247005-247008.
- Subedi, A., Zhang, L., Singh, D.J. & Du, M.H. (2008). Density functional study of FeS, FeSe, and FeTe: Electronic structure, magnetism, phonons, and superconductivity, *Physical Review B* Vol. 78: 134514-134519.
- Takahashi, H., Igawa, K., Arii, K., Kamihara, Y., Hirano, M. & Hosono, H. (2008). Superconductivity at 43 K in an iron-based layered compound $\text{LaO}_{1-x}\text{F}_x\text{FeAs}$. *Nature (London, United Kingdom)*, 453:376-378.
- Tamai, A., Ganin, A.Y., Rozbicki, Bacsá, E.J., Meevasana, W., King, P.D.C., Caffio, M., Schaub, R., Margadonna, S., Prassides, K., Rosseinsky, M.J. & Baumberger, F. (2010). Strong Electron Correlations in the Normal State of the Iron-Based $\text{FeSe}_{0.42}\text{Te}_{0.58}$ Superconductor Observed by Angle-Resolved Photoemission Spectroscopy. *Physical Review Letters*, 104:097002
- Wu, M.K., Hsu, F.C., Yeh, K.W., Huang, T.W., Luo, J.Y., Wang, M.J., Chang, H.H., Chen, T.K., Rao, S.M., Mok, B.H., Chen, C.L., Huang, Y.L., Ke, C.T., Wu, P.M., Chang, A.M., Wu, C.T. & Perng, T.P. (2009). The development of the superconducting PbO-type β -FeSe and related compounds. *Physica C*, 469 (9-12):340-349.
- Xu, G., Ming, W.M., Yao, Y.G., Dai, X., Zhang, S.C. & Fang, Z. (2008). Doping-dependent phase diagram of LaOMAs ($M=\text{V}-\text{Cu}$) and electron-type superconductivity near ferromagnetic instability. *Europhysics Letters*, 82:67002.
- Yamasaki, A., Matsui, Y., Imada, S., Takase, K., Azuma, H., Muro, T., Kato, Y., Higashiya, A., Sekiyama, A., Suga, S., Yabashi, M., Tamasaku, K., Ishikawa, T., Terashima, K., Kobori, H., Sugimura, A., Umeyama, N., Sato, H., Hara, Y., Miyagawa, N. & Ikeda I. (2010). Electron correlation in the FeSe superconductor studied by bulk-sensitive photoemission spectroscopy. *Physical Review B*, 82: 184511.
- Yang, W.L., Sorini, A.P., Chen, C.-C., Moritz, B., Lee, W.-S., Vernay, F., Olalde-Velasco, P., Denlinger, J.D., Delley, B., Chu, J.-H., Analytis, J.G., Fisher, I.R., Ren, Z.A., Yang, J., Lu, W., Zhao, Z.X., van den Brink J., Hussain, Z., Shen, Z.-X. & Devereaux, T.P. (2009). Evidence for weak electronic correlations in iron pnictides. *Physical Review B*, 80:014508.
- Yeh, K.W., Huang, Z.W., Huang, Y. L., Chen, T. K., Hsu, F. C., Wu, P.M., Lee, Y. C., Chu, Y. Y., Chen, C. L., Luo, J. Y., Yan, D.C. & Wu, M.K. (2008). Tellurium substitution effect on superconductivity of the α -phase iron selenide. *Europhysics Letters*, 84:37002.
- Yeh, K.W., Ke, C.T., Huang, T.W., Chen, T.K., Huang, Y.L., Wu, P.M. & Wu, M.K. (2009). Superconducting $\text{FeSe}_{1-x}\text{Te}_x$ Single Crystals Grown by Optical Zone-Melting Technique. *Crystal Growth Design*, 9:4847.
- Yildirim, T. (2008). Origin of the 150-K anomaly in LaFeAsO : competing antiferromagnetic interactions, frustration, and a structural phase transition, *Physical Review Letters*, 101: 057010-057013.
- Yoshida, R., Wakita, T., Okazaki, H., Mizuguchi, Y., Tsuda, S., Takano, Y., Takeya, H., Hirata, K., Muro, T., Okawa, M., Ishizaka, K., Shin S., Harima, H., Hirai M., Muraoka, Y.

& Yokoya, T. (2009). Electronic Structure of Superconducting FeSe Studied by High-Resolution Photoemission Spectroscopy. *The Physical Society of Japan*, 78: 034708.

Zaanen, J., Sawatzky, G.A. & Allen, J.W. (1985). Band gaps and electronic structure of transition-metal compounds, *Physical Review Letters*, 55: 418-421.

IntechOpen

IntechOpen